International Journal of Civil Engineering

Structural Engineering

Size optimization of nonlinear scallop domes by an enhanced particle swarm algorithm

R. Kamyab[1,*], **E. Salajegheh**[2]

Received: September 2012, Accepted: December 2012

Abstract

The present paper focuses on size optimization of scallop domes subjected to static loading. As this type of space structures includes a large number of the structural elements, optimum design of such structures results in efficient structural configurations. In this paper, an efficient optimization algorithm is proposed by hybridizing particle swarm optimization (PSO) algorithm and cellular automata (CA) computational strategy, denoted as enhanced particle swarm optimization (EPSO) algorithm. In the EPSO, the particles are distributed on a small dimensioned grid and the artificial evolution is evolved by a new velocity updating equation. In the new equation, the difference between the design variable vector of each site and an average vector of its neighboring sites is added to the basic velocity updating equation. This new term decreases the probability of premature convergence and therefore increases the chance of finding the global optimum or near global optima. The optimization task is achieved by taking into account linear and nonlinear responses of the structure. In the optimization process considering nonlinear behaviour, the geometrical and material nonlinearity effects are included. The numerical results demonstrate that the optimization process considering nonlinear behaviour results in more efficient structures compared with the optimization process considering linear behaviour.

Keywords: *Optimization, Scallop domes, Particle swarm optimization, Cellular automata, Nonlinear behavior, Static loading.*

1. Introduction

As the space structures are employed to cover wide span column free areas, they have a huge number of structural elements and therefore, sufficient attention must be paid to systematic designing of these structures. For this purpose, design of space structures can be conveniently achieved by employing optimization techniques. It is obvious that an optimal design has a great influence on the economy and safety of all types of the structures. In this case, optimizing space structures results in more efficient structural configurations. The present study is devoted to design optimization of a specific type of space structures denoted as scallop domes [1]. Configuration of scallop domes includes alternate ridges and grooves that radiate from the centre. There are many actual examples of scallop domes which are constructed throughout the world.

In the recent years, much progress has been made in optimum design of space structures by considering linear behavior [2-7]. It is observed that some trusses have nonlinear behavior even in usual range of loading [7-9]. Therefore, neglecting nonlinear effects in design optimization of these structures may be led to uneconomic designs. In this study, scallop domes are designed for optimal weight considering linear and nonlinear behaviors. In this paper, optimization of scallop domes with linear and nonlinear behaviors are denoted as linear optimization and nonlinear optimization, respectively. In the case of nonlinear optimization, geometrical and material nonlinearity effects are taken into account. All of the structural optimization problems have two main phases: analysis and optimization. In the analysis phase, opensees [10] platform is employed. In the optimization phase, particle swarm optimization (PSO) [11] is utilized. PSO is a popular meta-heuristic optimization algorithm and many successful applications of it have been reported in the field of structural optimization during last years [12-16]. The main drawback of PSO is a slow rate of convergence which increases the computational burden of the optimization process. In the present study, a computational strategy is proposed to improve the computational performance of the PSO. In the proposed enhanced particle swarm optimization (EPSO) algorithm, the global search ability of the PSO is enhanced by

* *Corresponding Author: rkamyab@uk.ac.ir*
Department of Civil Engineering, Shahid Bahonar University of Kerman, Kerman, Iran.

employing the concept of cellular automata (CA) [17].

Basically, CA represents simple mathematical idealizations of physical systems in which space and time are discrete and physical quantities are taken from a finite set of discrete values. Models based on CA provide an alternative and more general approach to physical modeling rather than an approximation [18-19]. In the proposed EPSO, the particles are distributed on a small dimensioned grid and the artificial evolution is evolved by a new velocity updating equation. In which the velocity updating rule is defined by adding a new cellular automata based term to the conventional equation. The original PSO can not control the balance between exploration and exploitation [20]. The proposed EPSO eliminates this difficulty and also reduces the number of required structural analyses during the optimization process compared with the PSO algorithm.

All of the required programs are coded in MATLAB [21]. In this paper, the design variables are cross sectional areas of the structural elements. The design constraints involved here are nodal displacements and element stresses constraints for linear optimization, but serviceability checks (nodal displacements at service loads) are involved only for nonlinear one. Two illustrative examples presented and the numerical results reveal that the nonlinear optimization of scallop domes results in more efficient designs compared with the linear optimization.

2. Scallop Domes

2.1. The Idea of Scallop Domes

The idea of scallop domes was proposed for the first time by Nooshin et. al [1]. Consider the dome configuration, a perspective view of which is shown in Figure 1a. This is a single layer dome whose nodes lie on a spherical cap. The plan view of the dome is shown in Figure 1b [1]. Now, consider the dome configuration shown in Figure 1d. The plan view of this dome is identical to that of the dome of Figure 1a, as given in Figure 1b. Also, the borders of the segments in Figure 1d are identical in shape to the ones in Figure 1a. The difference between the domes of Figures 1a and 1d is that the segments in Figure 1d are arched.

More specifically, in the case of the dome in Figure 1d, the nodal points along every circumferential ring are raised vertically such that the part of the ring between the borders in each segment is turned into an arch. The arching effect is such that: The nodal points on the segmental borders remain in their original positions (in particular, the position of the crown of the dome remains unchanged) and the rise of the arches increases with distance from the crown of the dome. The maximum rise for a circumferential ring, which occurs at the middle of each segment, is referred to as the "amplitude of the ring". The ring that is furthest away from the crown, namely, the "base ring" has the largest amplitude. This amplitude is referred to as the "amplitude of the dome", as indicated in Figure 1d. In this figure, the dotted curve shows the identical position of the base ring before "arching" of the segments. The dome of Figure 1d is an example of a class of domes that are referred to as scallop domes [1].

2.2. Segmental Disposition

Further examples of scallop domes are shown in Figure 2. The dome configurations in Figures 2a and 2b are obtained by scalloping the dome in Figure 1a. The dome in Figure 2a has 12 arches segments and the dome in Figure 2b has 3 arched segments. In general, a scallop dome may have any number of arched segments. If the number of arched segments is n, then the dome is referred to as an n-segment scallop dome. Thus, the dome in Figure 2a is a 12-segment scallop dome and the dome in Figure 2b is a 3-segment scallop dome. The central angle (in plan) of the arched segments of a scallop dome is referred to as the gauge angle of the dome. The gauge angles of the scallop domes in Figure 2a and 2b are 30 and 120, respectively [1]. The scallop domes in Figures 1d and 1e have an important difference with the domes in Figures 2a and 2b. Namely, the borders of the arched segments of the domes in Figures 1d and 1e are coincident with the meridional ribs that subdivide the pattern of the initial dome in Figure 1a into identical sectors. In contrast, the arched segments of the scallop domes in Figures 2b do not have an exact correspondence with the sectors of the initial dome. In general, a segmental border in a scallop dome need not necessarily correspond to any particular feature of the pattern of the elements of the dome. Irrespective of such a correspondence, however, the shape of a segmental border will always remain unaffected by the scalloping process [1].

Another example of a scallop dome is shown in Figure 2d involving 9 arched segments with a gauge angle of 40. This dome is obtained by scalloping the dome in Figure 2c. The pattern of the dome elements in this example is different from that of the domes considered above. This brings out the point that the applicability of the scalloping process does not depend on the pattern of the elements. This is true because it is the surface of a dome which is subjected to the scalloping process

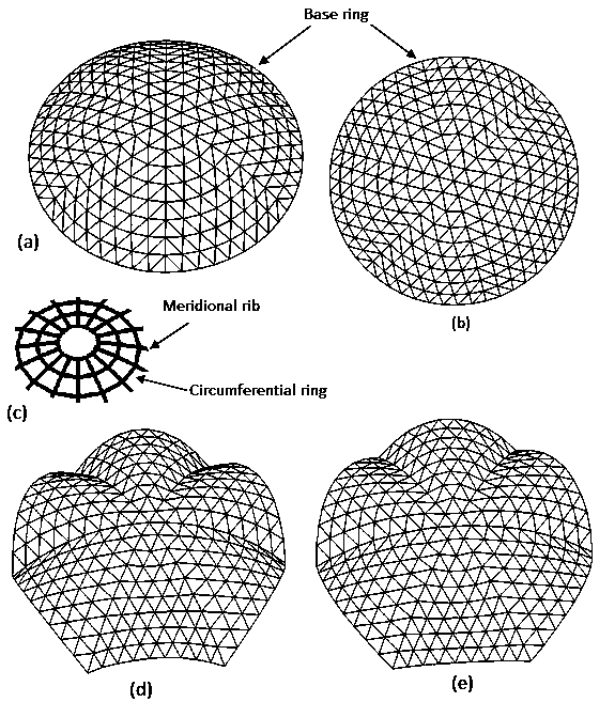

Fig. 1 Example of a scallop dome

and, therefore, any pattern on the surface will simply follow the transformation of the surface and the elements will assume the sizes and positions dictated by the nodal points.

3. Theoretical Background of Nonlinear Analysis

In a linear static analysis it is assumed that the deflections and strains are very small and the stresses are smaller than the material yield stresses. Consequently, the stiffness can be considered to independence of the displacements and forces and the finite element equilibrium equations are linear.

$$P=K\,\delta \tag{1}$$

where P, K and δ are the external load vector, stiffness matrix and nodal displacements vector, respectively.

This linearity implies that any increase or decrease in the load will produce proportional increase or decrease in displacements, strains and stresses. But it is clear that, in many structures, at or near failure (ultimate) loads, the deflections and the stresses do not change proportionately with the loads. Either the stresses are so high that they no longer obey Hooke's law or there are such large deflections that the compatibility equations to be linear. These two conditions are called material nonlinearity and geometric nonlinearity, respectively. In this study, a finite elements model based on geometrical and material nonlinear analyses of scallop domes including plasticity, and large deflection capabilities is presented by opensees. In this model a 3-D uniaxial co-rotational truss element is used. Flow rule in this model is associative and the hardening rule is Bi-linear kinematics hardening in tension. In compression, according to FEMA274 [22], it is assumed that the element buckles at its corresponding buckling stress state and its residual stress is about 20% of the buckling stress. In this case, the stress-strain relation shown in Figure 3 is employed in this study. In this figure, σ_b, σ_y and σ_u are buckling, yield and ultimate stresses, respectively and ε_b, ε_y and ε_u are their corresponding strains.

In the nonlinear structural analysis process, instead of the linear strain, a nonlinear one is used. Since the strains are nonlinear functions of the displacements or when the stresses reach values exceeding the yield stress of the material, the stress to strain relationship is nonlinear. In these cases, the stiffness is dependent on the displacements and the strains. Obviously, the solution of the displacements can not be obtained in a single step. Instead, the analysis is carried out by the incremental method combined with some iterative equilibrium corrections at every step [23]. In this work, the arch-length method of solution is used. The steps of the solution procedure are as follows:

1. Form tangent stiffness matrix (K_t) with the latest values of displacements and stresses.

$$\boldsymbol{K}_t = \sum_{1}^{N_e} \int_e \boldsymbol{B}_{nl}^{\mathrm{T}} \boldsymbol{D}_{ep} \boldsymbol{B}_{nl} d\,v \tag{2}$$

where D_{ep} is elasto-plastic material stiffness matrix and B_{nl} is the matrix that relates nonlinear strains to nonlinear nodal displacements.

2. The incremental displacements equation is solved:

$$\Delta\delta = K_t^{-1}(\Delta P + \psi) \tag{3}$$

where ΔP is part of load vector to be applied at the current increment and ψ is the residual force vector.

3. The incremental displacements are added to the total displacements:

$$\delta \rightarrow \delta + \Delta\delta \tag{4}$$

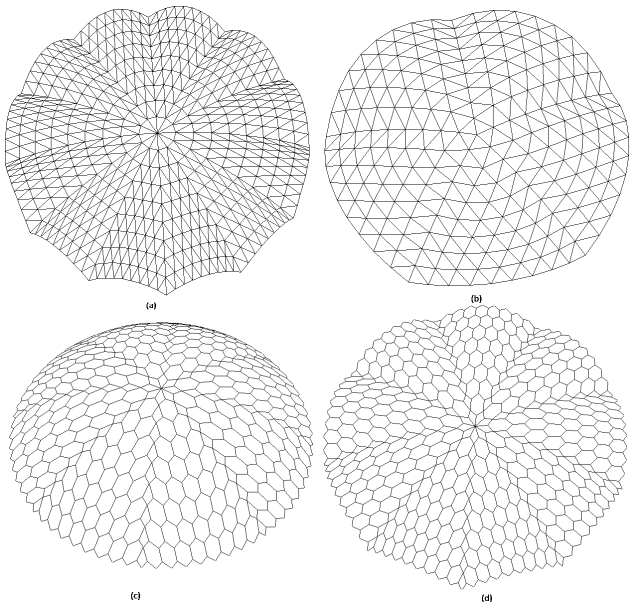

Fig. 2 More example of a scallop dome

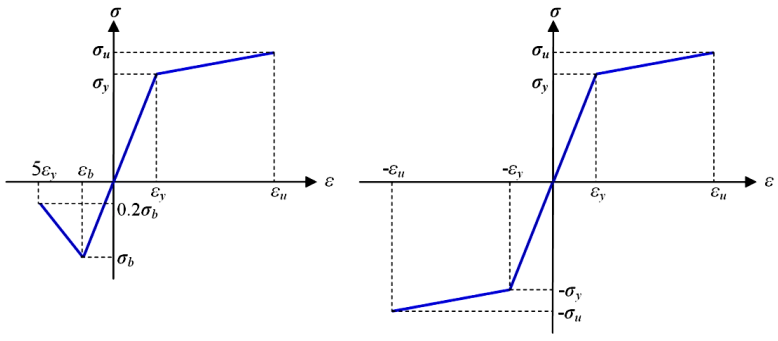

(a) (b)

Fig. 3 Stress-strain curve: (a) if $\sigma_b < \sigma_y$, (b) if $\sigma_b > \sigma_y$

4. The nonlinear strains are computed based on the latest estimate of the the incremental strains $\Delta\varepsilon$.

5. Total stresses are computed using the linear elastic stress strain relation:

$$\sigma \rightarrow \sigma + D\Delta\varepsilon \tag{5}$$

where D is elastic material stiffness matrix.

6. A check is performed to see if the estimated stresses are within the elastic limit: If the current point is plastic, then the computation is continued from step 7, else from step 8.

7. The elastic and plastic parts of the incremental strains are computed.

8. Contributions of the current Gauss point to the element internal forces are computed:

$$f_i = \int_e \boldsymbol{B}_{nl}^{\mathrm{T}} \sigma \, d\, v \tag{6}$$

9. Residual forces are computed:

$$\psi = \sum_{i=1}^{n_e} (f_i - F) \tag{7}$$

where F contains the external forces and n_e is the number of elements.

10. Incremental loads are applied at the next increment and steps 1 to 9 are repeated until convergence.

To increase the speed and accuracy of the nonlinear analysis, the applied loads are segmented into some loads termed sub-steps and then, in each sub-step arch-length method is used.

4. Formulation of Optimization Problem

It is shown that consideration of nonlinear behavior in the optimum design of structures not only provides more realistic results, but also produces lighter structures [8-9]. Nonlinear structural behavior arises from a number of causes, which can be grouped into geometrical and material nonlinearity. If a structure experiences large deformations, its changing geometric configuration can cause the structure to respond nonlinearly. Nonlinear stress-strain relationships are a common cause of material nonlinear behavior. One of the main factors that can influence a material's properties is load history in elasto-plastic response.

4.1. Linear Optimization

In optimal design problem of linear scallop domes the aim is to minimize the weight of the structure under stress and displacement constraints at service loads. The linear optimization problem can be expressed as follows:

$$\text{Minimize: } w(X) = \sum_{t=1}^{ng} x_t \sum_{j=1}^{nm} \gamma_j l_j$$

$$\begin{aligned} \text{Subject to: } & g_{dj}(X) = \delta_j - \delta_{ju} \leqq 0 \,,\ j = 1,\ldots,p \\ & g_{sk}(X) = \sigma_k - \sigma_{ku} \leqq 0 \,,\ k = 1,\ldots,ne \end{aligned} \tag{8}$$

where x_t, γ_j and l_i are cross sectional area of members belonging to group t, weight density and length of jth element in this group, respectively; ng and nm are the total number of groups in the structure and the number of members in group n, respectively; δ_j and δ_{ju} is the displacement of jth joint and its upper bound, respectively; p is the number of the nodes. Also σ_k and σ_{ku} is the stress of kth member and its upper bound, respectively; ne is the total number of members.

In the case of linear optimization, the allowable tensile and compressive stresses are used according to the AISC ASD (1989) code [24] as follows:

$$\begin{cases} \sigma_{ka} = 0.6\sigma_y & \text{for tensile stress} \\ \sigma_{ka} = \sigma_{cr} & \text{for compression stress} \end{cases} \tag{9}$$

$$\sigma_{cr} = \begin{cases} \left[(1 - \dfrac{\lambda_k^2}{2C_c^2})\sigma_y \right] \Big/ \left[\dfrac{5}{3} + \dfrac{3\lambda_k}{8C_c} - \dfrac{\lambda_k^3}{8C_c^3} \right] & \lambda_k < C_c \\ \dfrac{12\pi^2 E}{23\lambda_k^2} & \lambda_k \geq C_c \end{cases} \tag{10}$$

where E is the modulus of elasticity; F_y is the yield stress of steel; C_c is the slenderness ratio (λ_k) dividing the elastic and inelastic buckling regions ($C_c = \sqrt{2\pi^2 E/F_y}$); λ_k is the slenderness ratio ($\lambda_k = Kl_k/r_k$); K is the effective length factor; l_k is the member length and rk is the radius of gyration. In this case, linear analysis is employed although it was observed that there is not much difference between linear and geometry nonlinear analyses for service load.

4.2. Nonlinear Optimization

In the case of nonlinear optimization, design constraints include serviceability checks (nodal displacements at service loads) and stability constraints to ensure the stability of the scallop dome during the optimization process. The non linear optimization problem can be expressed as follows:

$$\text{Minimize: } w(X) = \sum_{t=1}^{ng} x_t \sum_{j=1}^{nm} \gamma_j l_j$$

$$\begin{aligned} \text{Subject to: } & g_{dj}(X) = \delta_j - \delta_{ju} \leqq 0 \,,\ j = 1,\ldots,p \,,\ \textit{at service load} \\ & g_f(X) = f_a - f_u \leqq 0 \\ & g_{sk}(X) = \sigma_k - \sigma_{ku} \leqq 0 \,,\ k = 1,\ldots,ne \end{aligned} \tag{11}$$

where f_a is applied load and f_u is ultimate load determined by using nonlinear analysis. Also σ_k and σ_u is the stress of kth member and ultimate stress, respectively, which are determined by using figure 3. In addition, the material and geometry nonlinear analyses are used in this case.

5. Particle Swarm Optimization

In structural optimization problems, where the objective function and the constraints are highly non-linear functions of the design variables, the computational effort spent in gradient calculations required by the mathematical programming algorithms is usually large. In recent years, it was found that probabilistic search algorithms are computationally efficient even if greater number of optimization cycles is needed to reach the optimum. Furthermore, probabilistic methodologies were found to be more robust in finding the global optima, due to their random search, whereas mathematical programming algorithms may be trapped into local optima. In the present

study, PSO is used.

The PSO has been inspired by the social behaviour of animals such as fish schooling, insect swarming and bird flocking. The PSO involves a number of particles, which are randomly initialized in the search space of an objective function. These particles are referred to as swarm. Each particle of the swarm represents a potential solution of the optimization problem. The particles fly through the search space and their positions are updated based on the best position of individual particles in each iteration. The objective function is evaluated for each particle to determine the best position in the search space. In iteration k, the swarm is updated using the following equations:

$$V_i^{k+1}=\omega^k V_i^k + c_1 r_1 (P_i^k - X_i^k) + c_2 r_2 (P_g^k - X_i^k) \quad (12)$$

$$X_i^{k+1} = X_i^k + V_i^{k+1} \quad (13)$$

$$\omega = \omega_{max} - \frac{\omega_{max} - \omega_{min}}{T_{max}} . T \quad (14)$$

where X_i and V_i represent the current position and the velocity of the ith particle, respectively; P_i is the best previous position of the ith particle (called pbest) and P_g is the best global position among all the particles in the swarm (called gbest); r_1 and r_2 are two uniform random sequences generated from interval [0, 1]; c_1 and c_2 are the cognitive and social scaling parameters, respectively. The inertia weight used to discount the previous velocity of particle preserved is expressed by ω. Also ω_{max} and ω_{min} are the maximum and minimum values of ω, respectively; T_{max}, and T are the numbers of maximum and current iterations, respectively.

The type of exploration mechanism of PSO enables the algorithm to solve many optimization problems spending low computational cost compared with other meta-heuristics. However, in the case of large scale optimization problems, implementation of PSO is usually confronted with difficulties such as escaping from the local optima which decreases the possibility of finding global optimum. In this paper, the computational advantages of the CA are utilized in order to mitigate the difficulties of PSO in the case of size optimization of nonlinear scallop domes. In the next section, the fundamental concepts of CA are briefly explained.

6. Cellular Automata

Cellular automata (CA) were firstly introduced by Von Neumann [17] and subsequently developed by other researchers in many fields of science. Basically, CA represents simple mathematical idealizations of physical systems in which space and time are discrete, and physical quantities are taken from a finite set of discrete values. Models based on CA provide an alternative and more general approach to physical modeling rather than an approximation. The CA shows a complex behavior analogous to that associated with complex differential equations, but in this case complexity emerges from the interaction of simple entities following simple rules [18].

In its basic form, a cellular automaton consists of a regular uniform grid of sites or cells with a discrete variable in each cell which can take on a finite number of states. The state of the cellular automaton is then completely specified by the values $s_i=s_i(t)$ of the variables at each cell i. During time, cellular automata evolve in discrete time steps according to a parallel state transition determined by a set of local rules: the variables $s_i^{k+1}=s_i(t_{k+1})$ at each site i at time t_{k+1} are updated synchronously based on the values of the variables $s_{n_c}^k$ in their n_c neighborhood at the preceding time instant t_k. The neighborhood n_c of a cell i is typically taken to be the cell itself and a set of adjacent cells within a given radius r; $i-r \leqq n_c \leqq i+r$. Thus, the dynamics of a cellular automaton can be formally represented as follows [25]:

$$s_i^{k+1} = \theta(s_i^k, s_{n_c}^k), \quad i-r \le n_c \le i+r \quad (15)$$

where the function θ is the evolutionary rule of the automaton.

One of the most important features of CA is the neighborhood structure. For updating the value of a cell, its own value and the values of neighboring cells should be considered. Configuration of the neighborhood structure is highly problem dependent and depends on the nature of the physical phenomenon that should be modeled. Clearly, a proper choice of the neighborhood plays a crucial role in determining the effectiveness of such a rule. In this paper, the widely used Moore neighborhood of interaction [25], by $r=1$, is adopted as shown in Figure 4. In this figure, the Moore neighborhood of the central cell is shown by gray region.

7. Enhanced Particle Swarm Optimization

In the recent years, many researchers have attempted to improve the computational performance of PSO algorithm. The followed computational strategies in this regard include two main classes. In the first class, researchers have combined PSO with the other optimization algorithms. For examples, two such optimization algorithms have been proposed by Gholizadeh and Salajegheh [26] and Kaveh and Talatahari [13]. In the second class, basic velocity equation of the standard PSO has been enhanced by adding some additional terms to it. As an example, Li et al. [12] proposed such modified equation. In the present paper, following the idea of the second class to discover a novel optimization mechanism through simulation of a social model, a new term is added to basic velocity equation of the standard PSO based on concepts of CA. The CA technique can be combined with the evolutionary algorithms to solve numerical optimization problems. In the field of structural optimization, Canyurt and Hajela [27], Rajasekaran [28], Salajegheh and Gholizadeh [29]

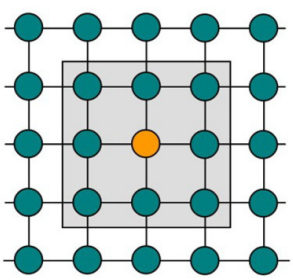

Fig. 4 Moore neighborhood

and Gholizadeh [30] have combined the concepts of CA and genetic algorithm (GA) to create cellular genetic algorithms (CGA). Also, Gholizadeh [18] has combined CA and PSO to optimize a number of benchmark linear structural optimization problems.

In the present paper CA and PSO are integrated and a cellular automata-based PSO algorithm is proposed to optimal design of linear and nonlinear scallop domes. In the proposed EPSO algorithm, particles are distributed on discrete locations of a 2D rectangular grid. The state variables associated with each cell site are simply the design variables of the optimization problem. In the traditional PSO, the particles' velocity and position in the search space is updated by applying Eqs. (12) to (14). In the EPSO, the updating process is accomplished based on a rule of the automaton. In this case, in the search process besides the global information, the local information of the Moor neighborhood of each central site is used to efficiently update its position in the design space. When the swarm has been updated, the evolutionary rules of the automaton are repeated until one of the stopping criteria is met. In both the PSO and EPSO, the objective function of the optimization problem is employed to define the fitness of each design vector. In this paper, a new velocity updating equation is presented.

In the proposed EPSO algorithm, a swarm of potential designs is structured on a 2D grid. In this case, each site contains a real-valued vector describing of a design and therefore the state of the cellular automaton in each site is a design vector of design variables as follows:

$$s_i \to X_i = \begin{Bmatrix} x_1 \\ x_2 \\ \vdots \\ x_n \end{Bmatrix}, i = 1,2,...,n_c \tag{16}$$

The proposed cellular velocity updating equation acts on the design variables and combines the global information (pbest and gbest) and the information available at the central site and its immediate neighbors as follows:

$$V_i^{k+1} = \omega^k V_i^k + c_1 r_1 (P_i^k - X_i^k) + c_2 r_2 (P_g^k - X_i^k) + c_3 r_3 (\frac{1}{n_c} \sum_{j=1}^{n_c} (X_{i,j}) - X_i^k) \tag{17}$$

where r_3 is a uniform random number generated from interval [0, 1]; c_3 is a scaling parameter. $X_{i,j}$ is the jth particle in immediate neighbors of ith central cell.

In each iteration or in each discrete time step, the proposed equation produces a new design at each site according to the following equation:

$$s_i^{k+1} = \theta(s_i^k, s_{n_c}^k) \to X_i^{k+1} = X_i^k + V_i^{k+1} \tag{18}$$

$$X_i^{k+1} = X_i^k + \omega^k V_i^k + c_1 r_1 (P_i^k - X_i^k) + c_2 r_2 (P_g^k - X_i^k) + c_3 r_3 (\frac{1}{n_c} \sum_{j=1}^{n_c} (X_{i,j}) - X_i^k) \tag{19}$$

In comparison with Eq. (12) of standard PSO algorithm, Eq. (19) in EPSO uses more information to update the velocity of particles. In this case, the difference between the design variable vector of each site and an average vector of design variables associated to its neighboring sites is added to the basic velocity updating equation. This new term decreases the probability of premature convergence to the gbest and therefore increases the chance of finding the global optimum or near global optima.

In [18], another CA based term was added to Eq. (12) and improved PSO was proposed for linear optimization of truss structures. In the present study, the mentioned improved PSO is used for nonlinear optimization of scallop domes and it is observed that the EPSO converges to better solutions compared with the mentioned improved PSO. Therefore, in this work for brevity the results of EPSO are compared only with those of standard PSO.

The values of algorithm parameters, ω_{min}, ω_{max}, c_1, c_2 and c_3 can seriously affect the computational performance of the EPSO algorithm. A sensitivity analysis is performed and the results reveal that the best values of the parameters are as follows: $\omega_{max} = 0.9$, $\omega_{min} = 0.4$, $c_1 = 1.0$, $c_2 = 2.0$ and $c_3 = 1.0$.

The flowchart of the proposed EPSO algorithm is shown in Figure 5.

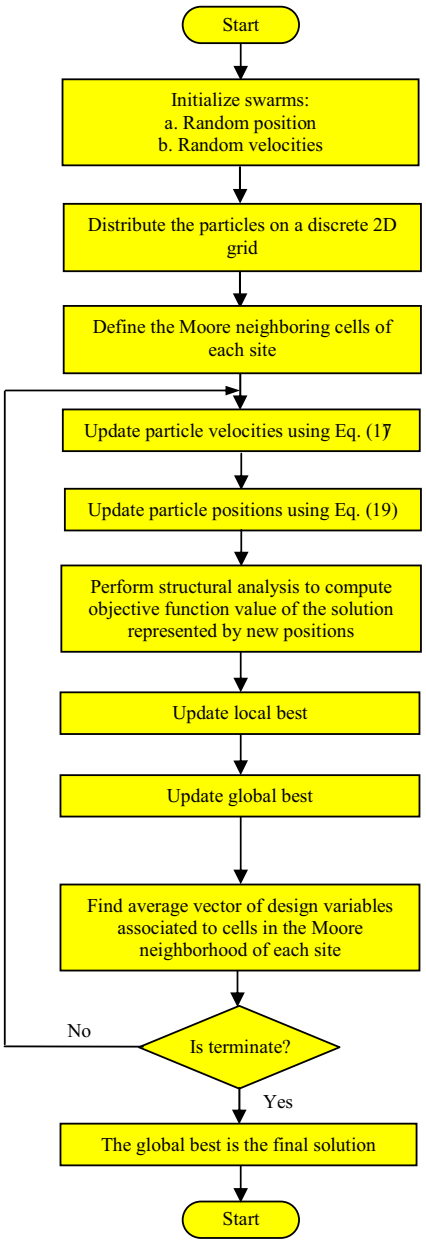

Fig. 5 Flowchart of the proposed EPSO algorithm

8. Numerical Results

In the present work, two double layer scallop domes with 8 and 10 segments are considered. For both the scallop domes the span is 50.0 m, the height is 10 m and the layer thicknesses is 1.5 m. The configuration of the mentioned scallop domes is shown in Figure 6. Young's modulus, mass density, yield stress and ultimate stress are 2.1×10^{10} kg/m2 (205.9 GPa), 7850 kg/m3 (76.98 kN/m^3), 2.4×10^6 kg/m^2 (235.4 MPa), and 3.6×10^6 kg/m^2 (353.0 MPa), respectively. The computational time is measured in terms of CPU time of a PC Pentium IV 3000 MHz. A uniformly distributed load of 250 kg/m^2 (2.4517 kN/m^2) is applied on the horizontal projection of the top layer.

The number of particles for PSO is 25 and for EPSO the same number of particles is distributed on a 5x5 discrete grid. The maximum number of iterations for both algorithms is limited to 400. For linear optimization, the stress constraints are checked according to Eqs (9) to (10) and the allowable vertical deflection is 5.00 cm. For nonlinear optimization, the constraints of Eq (11) are taken in to account. In the linear optimization process, the factors of safety (FS) is applied on the element tensile and compressive stresses as given by Eqs (9) and (10), respectively. For nonlinear optimization, FS is applied on the external loads. In this case, by considering FSs of 1.6 and 2.0, the scallop domes are optimized to bear the external loads of 400 kg/m^2 (3.9227 kN/m^2) and 500 kg/m^2 (4.9033 kN/m^2) while their corresponding maximum deflection at the service load (2.4517 kN/m^2) are limited to 5 cm. The discrete design variables are selected from a set of standard Pipe profiles listed in Table 1. In this table, cross-sectional area and radius of Gyration are given by A and r, respectively.

For all examples, the structural elements of each layer are divided into three groups and therefore the optimization problem includes nine design variables:

$$X^T=\{A_{Group1},A_{Group2},A_{Group3},A_{Group4},A_{Group5},A_{Group6},A_{Group7},A_{Group8},A_{Group9}\} \quad (20)$$

During the nonlinear optimization process, for each element a strain-stress curve is considered according to its buckling stress. It is important to note that for all structural elements σ_y, σ_u and their corresponding strains are identical.

8.1. Example 1: A 1200-bar 8-Segment Double Layer Scallop Dome

The plane views of the 8-segment scallop dome together with its element groups are shown in Figure 7.

The optimization task considering linear and nonlinear behaviors are achieved using PSO and EPSO algorithms and the results are given in Table 2.

In the case of linear optimization for service load of 250 kg/m^2 (2.4517 kN/m^2), the optimal weight corresponding to EPSO is 4.86% better than that of the PSO. For nonlinear optimization processes for ultimate loads of 400 kg/m^2 (3.9227 kN/m^2) and 500 kg/m^2 (4.9033 kN/m^2), the EPSO converges to solutions which are 4.75% and 4.32% lighter than solutions found by PSO. Also in the all cases, EPSO requires less generations compared with the PSO. The results show that, the computational performance of the EPSO is better than that of the PSO in terms of optimal weight and number of required generations.

The stresses of the critical elements in the nine groups of the optimum designs found by EPSO are compared with their corresponding upper bound values in Table 3.

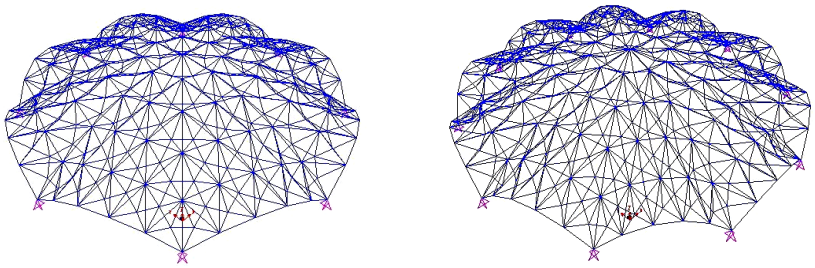

Fig. 6 Double layer scallop dome with (a) 8 and (b) 10 segments

Table 1 The available list of standard Pipe profiles (TUBO-)

NO.	Profile	A (cm^2)	r (cm)	NO.	Profile	A (cm^2)	r (cm)
1	D33.70x2.6	2.540	1.1000	14	D159.0x4.0	19.480	5.4814
2	D48.30x2.6	3.730	1.6200	15	D168.3x4.0	20.65	5.8102
3	D60.30x3.2	5.740	2.0200	16	D193.7x4.5	26.75	6.6922
4	D76.10x3.2	7.329	2.5799	17	D219.1x5.0	33.63	7.5716
5	D82.50x3.2	7.972	2.8060	18	D244.5x5.4	40.56	8.4557
6	D88.90x3.2	8.616	3.0321	19	D273.0x5.6	47.04	9.4570
7	D101.6x3.6	11.080	3.4672	20	D298.5x5.9	54.23	10.3471
8	D108.0x3.6	11.810	3.6934	21	D323.9x5.9	58.94	11.2450
9	D114.3x3.6	12.520	3.9161	22	D355.6x6.3	69.13	12.3536
10	D127.0x4.0	15.450	4.3504	23	D368.0x6.3	71.59	12.7895
11	D133.0x4.0	16.210	4.5629	24	D406.4x6.3	79.19	14.1475
12	D139.7x4.0	17.050	4.8004	25	D419.0x7.1	91.88	14.5645
13	D152.4x4.0	18.650	5.2483	26	D457.2x7.1	100.4	15.9150

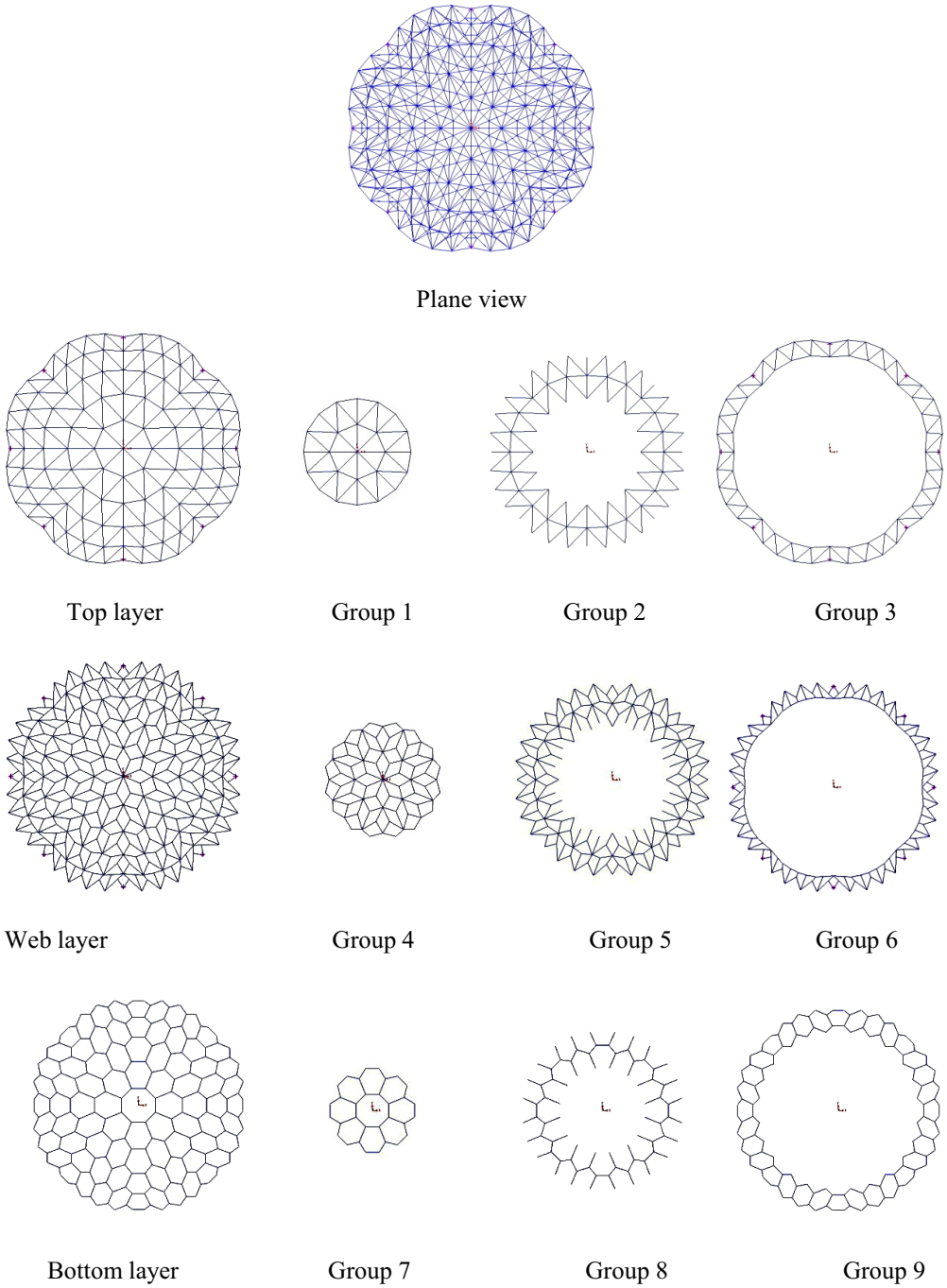

Fig. 7 The 8-segment scallop dome with its relative element groups

Table 2 Comparison of linear and nonlinear optimal designs found by PSO and EPSO

Design variables	Linear (Service load of 250 kg/m^2)		Nonlinear (Ultimate load of 400 kg/m^2)		Nonlinear (Ultimate load of 500 kg/m^2)	
	PSO	EPSO	PSO	EPSO	PSO	EPSO
A_{Group1}	D159.0x4.0	D159.0x4.0	D133.0x4.0	D159.0x4.0	D133.0x4.0	D114.3x3.6
A_{Group2}	D193.7x4.5	D168.3x4.0	D127.0x4.0	D114.3x3.6	D139.7x4.0	D88.90x3.2
A_{Group3}	D244.5x5.4	D219.1x5.0	D193.7x4.5	D193.7x4.5	D193.7x4.5	D219.1x5.0
A_{Group4}	D76.10x3.2	D60.30x3.2	D60.30x3.2	D60.30x3.2	D82.50x3.2	D76.10x3.2
A_{Group5}	D82.50x3.2	D88.90x3.2	D101.6x3.6	D88.90x3.2	D101.6x3.6	D101.6x3.6
A_{Group6}	D127.0x4.0	D168.3x4.0	D108.0x3.6	D101.6x3.6	D133.0x4.0	D114.3x3.6
A_{Group7}	D76.10x3.2	D76.10x3.2	D133.0x4.0	D127.0x4.0	D159.0x4.0	D193.7x4.5
A_{Group8}	D82.50x3.2	D82.50x3.2	D82.50x3.2	D101.6x3.6	D114.3x3.6	D127.0x4.0
A_{Group9}	D127.0x4.0	D152.4x4.0	D88.90x3.2	D88.90x3.2	D127.0x4.0	D127.0x4.0
Weight (kN)	624.633	594.296	467.86	445.58	540.282	516.919
Number of generations	200	192	196	178	197	165
Overall time (min.)	62.00	59.50	465.34	426.92	470.87	389.58
Max. deflection at service load (cm)	3.09	3.04	4.11	3.90	3.85	3.89

Numerical results demonstrate that all of the found optimum designs are feasible. It is important to note that by taking into account nonlinear behaviour of the scallop domes the structural weight can be considerably reduced compared with the linear one.

Convergence histories of the linear optimization processes, for service load of 250 kg/m^2 (2.4517 kN/m^2), are compared with those of the nonlinear optimization processes, for ultimate loads of 400 kg/m^2 (3.9227 kN/m^2) and 500 kg/m^2 (4.9033 kN/m^2), in Figure 8 for PSO and EPSO algorithms.

The load-deflection diagram of the top node of the optimum scallop domes found by EPSO for ultimate loads is also shown in Figure 9.

Also, for the nonlinear optimum design subject to ultimate load of 500 kg/m^2 (4.9033 kN/m^2), the incremental distributed load-vertical displacement curves of a number of selective nodes are shown in Figure 10.

The results show that the nonlinear optimization process, for ultimate load of 500 kg/m^2 (4.9033 kN/m^2), converges to a

Table 3 Stresses of the critical elements in the nine groups of the optimum designs found by EPSO

Group NO.	Linear stresses (MPa) for service load of 250 kg/m^2			σ^+_{all}	Nonlinear Stresses (MPa) For ultimate load of 400 kg/m^2			For ultimate load of 500 kg/m^2			σ_u
	σ^-	σ^-_{all}	σ^+		σ^-	σ_b	σ^+	σ^-	σ_b	σ^+	
1	-82.69	-87.71	-	141.2	-136.96	-200.98	-	-101.89	-102.59	-	353.0
2	-91.89	-92.06	10.22	141.2	-102.48	-102.59	35.23	-105.83	-107.32	75.59	353.0
3	-105.03	-107.51	9.78	141.2	-239.90	-353.01	27.15	-261.37	-353.02	60.65	353.0
4	-44.64	-58.95	39.65	141.2	-96.63	-113.00	78.59	-122.72	-130.76	67.37	353.0
5	-53.62	-87.21	77.41	141.2	-206.84	-235.34	199.08	-157.43	-235.34	226.50	353.0
6	-92.69	-121.08	50.86	141.2	-243.48	-353.01	133.76	-287.64	-353.02	151.71	353.0
7	-65.94	-84.67	11.54	141.2	-65.94	-235.34	16.38	-218.13	-235.34	-	353.0
8	-68.29	-70.69	24.21	141.2	-116.09	-227.20	36.52	-212.60	-235.34	25.26	353.0
9	-81.86	-120.61	49.44	141.2	-171.94	-177.67	162.44	-236.02	-353.02	82.77	353.0

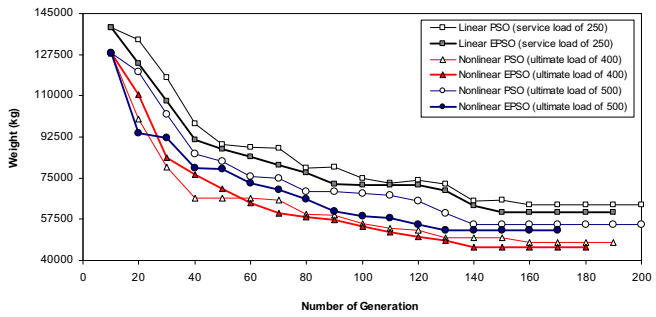

Fig. 8 The convergence history of the linear optimization process (for service load of 250 kg/m^2) and nonlinear optimization processes (for ultimate loads of 400 and 500 kg/m^2) for the first example

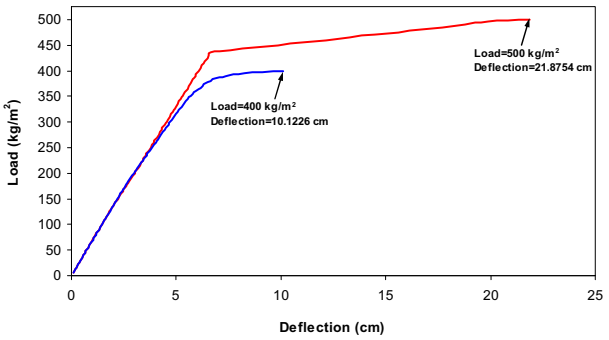

Fig. 9 Nonlinear deflection of the top node of the 8 segmented scallop domes for ultimate loads

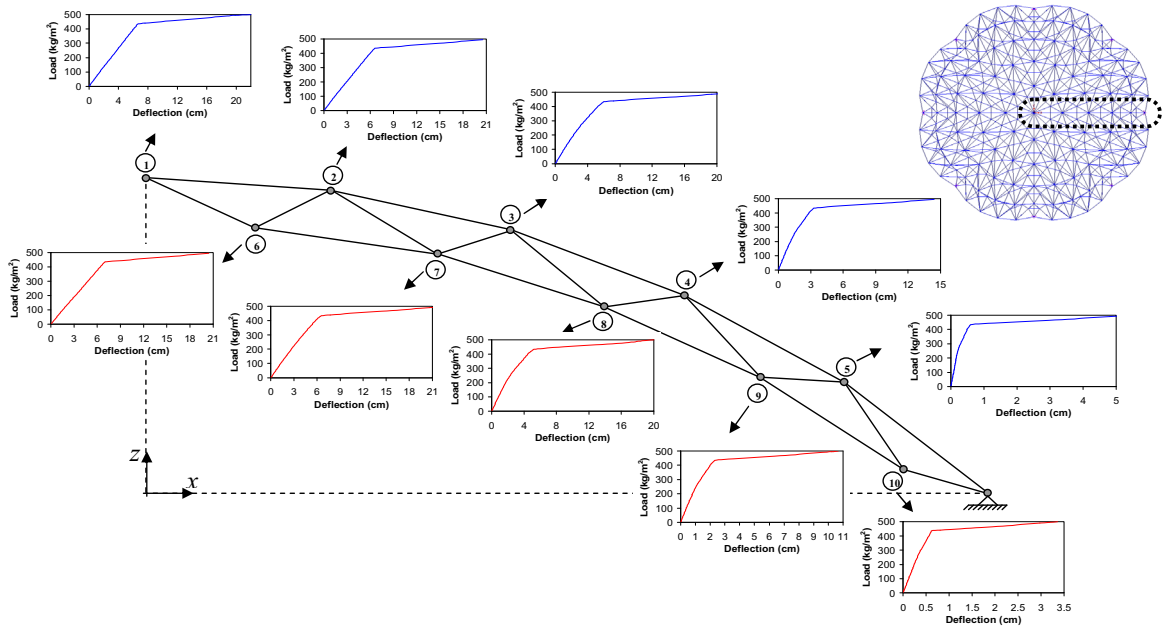

Fig. 10 Nonlinear deflection of the top and bottom layers' nodes of the shown part of the optimum 8 segmented scallop dome subject to ultimate load of 500 kg/m^2

solution with the weight of 516.919 kN which is lighter than 594.296 kN (13.02%) of the linear optimization process, for service load, while the FS of former (2.0) is considerably larger than that of the later (about 1.6). These observations demonstrate that the by considering nonlinear behaviour of scallop domes it is possible to find designs having higher FS and lighter weight compared with linear optima.

8.2. Example 2: A 1500-bar 10-Segment Double Layer Scallop Dome

The plane views and element groups of the 10-segment scallop dome are shown in Figure 11.

The results of optimization using PSO and EPSO algorithms considering linear and nonlinear behaviors are given in Table 4.

In the case of linear optimization the optimal weight found by EPSO is 4.51% lighter than that of the PSO. For nonlinear optimization processes subject to ultimate loads of 400 kg/m^2 (3.9227 kN/m^2) and 500 kg/m^2 (4.9033 kN/m^2), the EPSO converges to solutions which are 4.32% and 5.74% lighter than solutions found by PSO. Also in the all cases, EPSO requires less generations compared with the PSO. The results show that, the computational performance of the EPSO is better than that of the PSO in terms of optimal weight and number of required generations.

The stresses of the critical elements in the nine groups of the optimum designs found by EPSO are compared with their corresponding upper bound values in Table 5.

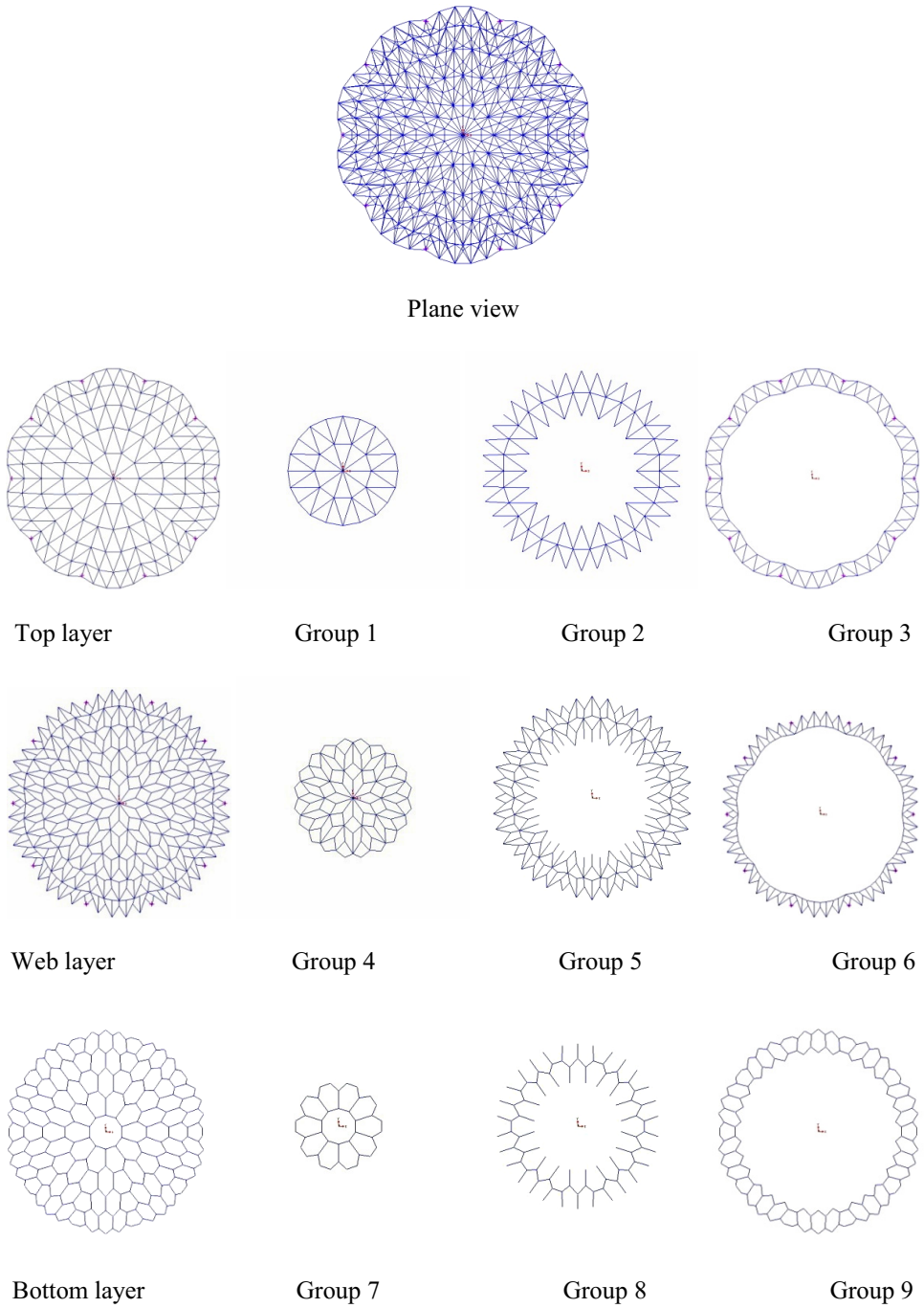

Fig. 11 The 10-segment scallop dome with its relative element groups

Table 4 Comparison of linear and nonlinear optimal designs found by PSO and EPSO

Design variables	Linear (Service load of 250 kg/m^2)		Nonlinear (Ultimate load of 400 kg/m^2)		Nonlinear (Ultimate load of 500 kg/m^2)	
	PSO	EPSO	PSO	EPSO	PSO	EPSO
A_{Group1}	D159.0x4.0	D152.4x4.0	D127.0x4.0	D127.0x4.0	D127.0x4.0	D133.0x4.0
A_{Group2}	D159.0x4.0	D159.0x4.0	D114.3x3.6	D108.0x3.6	D127.0x4.0	D114.3x3.6
A_{Group3}	D219.1x5.0	D193.7x4.5	D168.3x4.0	D159.0x4.0	D193.7x4.5	D193.7x4.5
A_{Group4}	D60.30x3.2	D60.30x3.2	D60.30x3.2	D60.30x3.2	D60.30x3.2	D60.30x3.2
A_{Group5}	D82.50x3.2	D76.10x3.2	D76.10x3.2	D76.10x3.2	D76.10x3.2	D76.10x3.2
A_{Group6}	D114.3x3.6	D133.0x4.0	D114.3x3.6	D108.0x3.6	D108.0x3.6	D108.0x3.6
A_{Group7}	D82.50x3.2	D76.10x3.2	D76.10x3.2	D76.10x3.2	D114.3x3.6	D101.6x3.6
A_{Group8}	D76.10x3.2	D76.10x3.2	D82.50x3.2	D76.10x3.2	D108.0x3.6	D101.6x3.6
A_{Group9}	D88.90x3.2	D88.90x3.2	D88.90x3.2	D82.50x3.2	D108.0x3.6	D88.90x3.2
Weight (kN)	587.298	560.794	452.844	433.269	528.179	497.821
Number of generations	200	198	185	168	183	162
Overall time (min.)	63.50	61.22	698.34	625.11	690.02	611.45
Max. deflection at service load (cm)	2.51	2.53	2.96	2.58	2.72	2.55

Table 5 Stresses of the critical elements in the nine groups of the optimum designs found by EPSO

Group NO.	Linear stresses (MPa) for service load of 250 kg/m^2			σ^+_{all}	Nonlinear Stresses (MPa) For ultimate load of 400 kg/m^2			For ultimate load of 500 kg/m^2			σ_u
	σ^-	σ^-_{all}	σ^+		σ^-	σ_b	σ^+	σ^-	σ_b	σ^+	
1	-80.09	-84.19	-	141.2	-120.01	-126.60	-	-138.71	-139.27	-	353.0
2	-83.07	-87.71	8.48	141.2	-89.57	-91.25	2.83	-102.31	-102.59	9.04	353.0
3	-100.13	-101.08	6.90	141.2	-197.80	-235.34	14.05	-225.64	-235.34	9.57	353.0
4	-49.39	-66.18	36.62	141.2	-96.43	-127.58	71.51	-121.44	-127.58	49.16	353.0
5	-47.41	-58.49	66.05	141.2	-141.06	-195.30	118.94	-111.32	-112.12	201.29	353.0
6	-90.55	-114.69	47.29	141.2	-221.31	-235.34	115.99	-235.17	-235.34	123.40	353.0
7	-98.04	-99.72	13.47	141.2	-182.37	-235.34	16.39	-210.81	-235.34	-	353.0
8	-45.93	-62.61	27.82	141.2	-113.89	-125.79	45.82	-115.33	-216.83	10.12	353.0
9	-99.68	-100.25	91.95	141.2	-217.06	-235.34	159.37	-221.16	-235.34	141.58	353.0

Numerical results demonstrate the feasibility of all of the found optimum designs. It is shown that by taking into account nonlinear behaviour of the scallop domes the structural weight can be considerably reduced compared with the linear one.

Convergence histories of the linear optimization processes are compared with those of the nonlinear optimization processes in Figure 12 for PSO and EPSO algorithms.

Also the load-deflection diagram of the top node of the optimum scallop domes found by EPSO for ultimate loads is shown in Figure 13.

As well as the first example, for the nonlinear optimum design subject to ultimate load of 500 kg/m^2 (4.9033 kN/m^2), the incremental distributed load-vertical displacement curves of a number of selective nodes are shown in Figure 14.

The results show that the nonlinear optimization process using EPSO, for ultimate load of 500 kg/m^2 (4.9033 kN/m^2), converges to a solution which is 11.23% lighter than that of the linear optimization process, for service load, while the FS of former is considerably larger than that of the later. This implies that by considering nonlinear behaviour of scallop domes it is possible to find optimum designs having higher FS and lighter weight compared with linear optima.

9. Conclusions

The present study deals with size design optimization of scallop domes for static loading. The cross-sectional areas of the element groups are the design variables and the weight of the structure is the objective function of the optimization problem. Two optimization processes considering linear and nonlinear behavior of the structure are included. In the nonlinear optimization process, geometrical and material nonlinearities are involved. In the present work, PSO is selected as the optimizer and its computational performance is

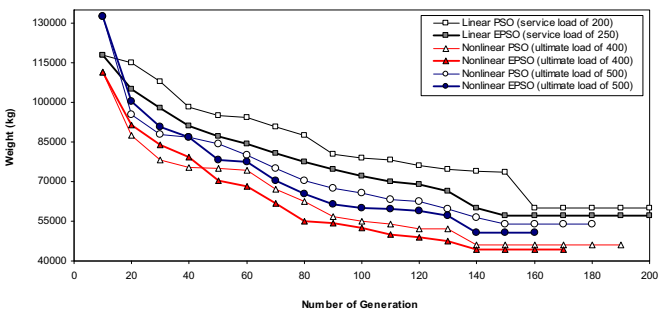

Fig. 12 The convergence history of the linear optimization process (for service load of 250 kg/m^2) and nonlinear optimization processes (for ultimate loads of 400 and 500 kg/m^2) for the second example

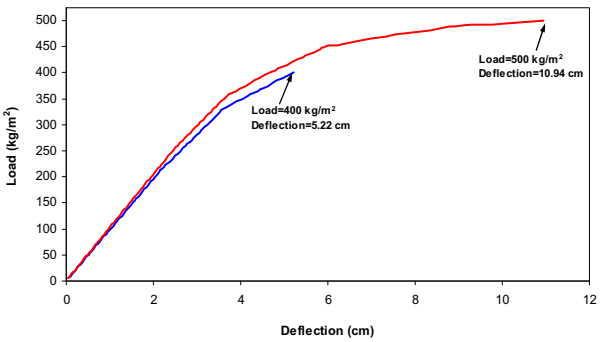

Fig. 13 Nonlinear deflection of the top node of the 10 segmented scallop domes for ultimate loads

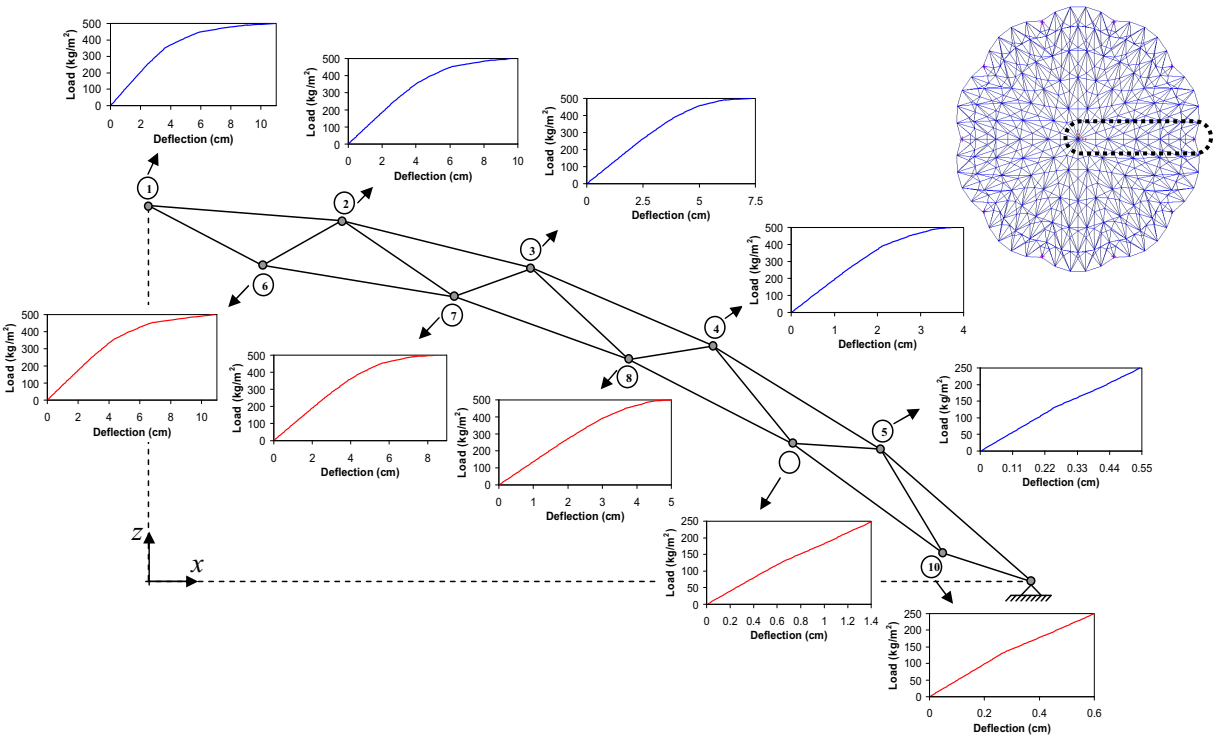

Fig. 14 Nonlinear deflection of the top and bottom layers' nodes of the shown part of the optimum 10 segmented scallop dome subject to ultimate load of 500 kg/m^2

improved using the concept of CA. The original PSO can not control the balance between exploration and exploitation. To eliminate this difficulty and also to reduce the number of required structural analyses during the optimization process, EPSO is proposed in this study. In the proposed EPSO, the particles are distributed on a small dimensioned grid and the artificial evolution is evolved by a new velocity updating equation. In which the velocity updating rule is defined by adding a new CA-based term to the conventional equation. In the sequel, an efficient optimization algorithm, denoted as EPSO, is consequently employed to achieve the difficult nonlinear optimization task. In the linear optimization process, stress and deflection constraints are checked and in the nonlinear optimization process the displacement constraints are considered at service load of 250 kg/m^2 (2.4517 kN/m^2) while the stability constraints are checked at the applied ultimate loads. In this paper, the factors of safety (FS) in the linear optimization process, is applied on the element tensile and compressive stresses, while for nonlinear optimization, FS is applied on the external loads. In this case, by considering FSs of 1.6 and 2.0, the scallop domes are optimized to bear the external loads of 400 kg/m2 (3.9227 kN/m^2) and 500 kg/m^2 (4.9033 kN/m^2).

The results show that, the computational performance of the EPSO is better than that of the PSO in terms of optimal weight and number of required generations. The numerical results also show that in all of the mentioned cases, the nonlinear optimization processes converge to solutions which are lighter than those of the linear optimization. This means that, considering nonlinear behaviour of scallop domes one can find optimum designs with higher FS and lighter weight compared with linear optimum designs.

References

[1] Nooshin H, Tomatsuri H, Fujimoto, M. Scallop domes. IASS97 Symposium on Shell & Spatial Structures: Design, Performance & Economics, Singapore, 1997.

[2] Gholizadeh S, Barzegar A. Shape optimization of structures for frequency constraints by sequential harmony search algorithm, Engineering Optimization, 2012; 45: 627-646

[3] Gholizadeh S, Salajegheh E, Torkzadeh P. Structural optimization with frequency constraints by genetic algorithm using wavelet radial basis function neural network, Journal of Sound and Vibration, 2008; 312: 316-331.

[4] Kaveh A, Farhmand Azar B, Talatahari S. Ant colony optimization for design of space trusses, International Journal of Space Structures, 2008; 23: 167-181.

[5] Gholizadeh S, Fattahi F. Design optimization of tall steel buildings by a modified particle swarm algorithm, The Structural Design of Tall and Special Buildings, 2012, DOI: 10.1002/tal.1042.

[6] Kaveh A, Talatahari S. Size optimization of space trusses using Big Bang-Big Crunch algorithm, Computers and Structures, 2009; 87: 1129–1140.

[7] Optimal design of barrel vaults using charged search system Ali Kaveh, Mahdi Sagharjooghifarahani, Nasim Shojaei, International Journal of Civil Engineering Volume 10, Number 4.

[8] Saka MP, Ulker M. Optimum design of geometrically nonlinear space trusses, Computers & Structures, 1991; 41: 1387-1396.

[9] Saka MP, Kameshki ES. Optimum design of nonlinear elastic framed domes, Advances in Engineering Software, 1998; 29: 519-528.

[10] McKenna F, Fenves G. The Opensees Command Language Manual, 1st ed., 2001.

[11] Eberhart RC, Kennedy J. A new optimizer using particle swarm theory, Proceedings of the Sixth International Symposium on Micro Machine and Human Science, Nagoya, Japan, 1995, pp. 39-43.

[12] Li LJ, Huang ZB, Liu F, Wu QH. A heuristic particle swarm optimizer for optimization of pin connected structures,

Computers and Structures, 2007; 85: 340–349.
[13] Kaveh A, Talatahari S. Particle swarm optimizer, ant colony strategy and harmony search scheme hybridized for optimization of truss structures, Computers and Structures, 2009; 87: 267–283.
[14] Gholizadeh S, Salajegheh E. Optimal design of structures for time history loading by swarm intelligence and an advanced metamodel, Computer Methods in Applied Mechanics and Engineering, 2009; 198: 2936–2949.
[15] Optimal design and operation of irrigation pumping systems using particle swarm optimization algorithm M.H. Afshar, R. Rajabpour, International Journal of Civil Engineering Volume 5, Number 4.
[16] Gholizadeh S, Seyedpoor SM. Shape optimization of arch dams by metaheuristics and neural networks for frequency constraints, Scientia Iranica, 2011; 18: 1020-1027.
[17] Von Neumann J. Theory of self-reproducing automata, A. W. Burks, (Eds.), University of Illinois Press, Champaign, Ill, 1966.
[18] Gholizadeh S. Optimum design of structures by an improved particle swarm algorithm, Asian Journal of Civil Engineering, 2010; 11: 779–796.
[19] Topolgy Optimization of Structures using Cellular Automata with Constant Strain Triangles Ebrahim Sanaei, Mehdi Babaei, Volume 10, Number 3.
[20] Angeline P. Evolutionary optimization versus particle swarm optimization: philosophy and performance difference. Proceeding of the Evolutionary Programming Conference, San Diego, USA; 1998.
[21] The Language of Technical Computing. MATLAB. Math Works Inc, 2006.
[22] Federal Emergency Management Agency. NEHRP guidelines for the seismic rehabilitation of buildings, Rep. FEMA 273 (Guidelines) and 274 (Commentary), Washinton, DC, 1997.
[23] Crisfield MA. Non-Linear Finite Element Analysis of Solids and Structures, John Wiley & Sons, Volume 1: Essentials, Chichester, 1991.
[24] AISC: American Institute of Steel Construction, Manual of steel construction-allowable stress design, 9th ed. Chicago, IL; 1989.
[25] Biondini F, Bontempi F, Frangopol DM, Malerba PG. Cellular automata approach to durability analysis of concrete structures in aggressive environments, Journal of Structural Engineering, 2004; 130: 1724–1737.
[26] Gholizadeh S, Salajegheh E. Optimal seismic design of steel structures by an efficient soft computing based algorithm, Journal of Constructional Steel Research, 2010; 66: 85–95.
[27] Canyurt OE, Hajela P. A cellular framework for structural analysis and optimization, Computer Methods in Applied Mechanics and Engineering, 2005; 194: 3516–3534.
[28] Rajasekaran S. Optimization of large scale three dimensional reticulated structures using cellular genetics and neural networks, International Journal of Space Structures, 2001; 16: 315–324.
[29] Gholizadeh S, Salajegheh E. A Cellular Genetic Algorithm for Structural Optimisation, In B.H.V. Topping, J.M. Adam, F.J. Pallares, R. Bru, M.L. Romero, (Ed), Proceedings of the Tenth International Conference on Computational Structures Technology, DATE, Stirlingshire: Civil-Comp Press, 1-14, 2010.
[30] Gholizadeh S. Optimum Design of Structures for Earthquake Loading by a Cellular Evolutionary Algorithm and Neural Networks, In V. Plevris, C.C. Mitropoulou, N.D. Lagaros, (Editors), "Structural Seismic Design Optimization and Earthquake Engineering: Formulations and Applications", IGI Global, USA, Chapter 12, 306-322, 2012.